are related. In general, four-coordinate d^9 complexes are expected to be stereochemically nonrigid with relatively low barriers between several potential energy minima. Thus, we may expect a readily accessible pathway for intramolecular ligand exchange, consistent with the extremely rapid fluxionality observed in the acetylene cobalt radicals.

Acknowledgment is made to the donors of the Petroleum Research Fund, administered by the American Chemical Society, for partial support of this research both at Brown University and at the University of Otago. We are grateful to the National Science Foundation for assistance in the purchase of an ESR spectrometer by Brown University. We thank P. J. Krusic for helpful discussions and for his encouragement in this work and H. F. Klein for communicating the details of some ESR spectra.

Registry No. $(Ph_2C_2)Co(CO)_3$, 90219-71-9; $(t\text{-}Bu_2C_2)Co(CO)_3$, 90219-72-0; $(Ph_2C_2)Co(CO)_2P\text{-}n\text{-}Bu_3$, 90219-73-1; $(Ph_2C_2)Co(CO)_2P(c\text{-}C_6H_{11})_3$, 90219-74-2; $(Ph_2C_2)Co(CO)_2PPh_3$, 90219-75-3; $(Ph_2C_2)Co(CO)_2P(OMe)_3$, 90245-32-2; $(Ph_2C_2)Co(CO)_2P(OPh)_3$, 90219-76-4; $(Ph_2C_2)Co(CO)_2AsPh_3$, 90219-77-5; $(t\text{-}Bu_2C_2)Co(CO)_2P\text{-}n\text{-}Bu_3$, 90219-78-6; $(t\text{-}Bu_2C_2)Co(CO)_2P(OMe)_3$, 90219-79-7; $[CF_3C_2Si(CH_3)_3]Co(CO)[P(OMe)_3]_2$, 90219-80-0; $[(CF_3)_2C_2]Co(CO)[P(OMe)_3]_2$, 90219-81-1; $(Ph_2C_2)Co(CO)[P(OEt)_3]_2$, 90219-82-2; $(Ph_2C_2)Co(CO)[P(OMe)_3]_2$, 90219-83-3; $(Ph_2C_2)Co(CO)[Ph_2PCH_2CH_2PPh_2]$, 90219-84-4; $(Ph_2C_2)Co(CO)[Ph_2AsCH_2CH_2AsPh_2]$, 90219-85-5; $(Ph_2C_2)Co(CO)[Ph_2PCH_2CH_2AsPh_2]$, 90219-86-6; $[(CF_3)_2C_2]Co[P(OMe)_3]_3$, 90219-87-7; $(Ph_2C_2)Co[P(OMe)_3]_3$, 90219-88-8; $(Ph_2C_2)Co_2(CO)_6$, 14515-69-6; $(t\text{-}Bu_2C_2)Co_2(CO)_6$, 59687-97-7; $[(CF_3)_2C_2]Co_2(CO)_6$, 37685-63-5; $[CF_3C_2Si(CH_3)_3]Co_2(CO)_6$, 38599-40-5; $(Ph_2C_2)Co_4(CO)_{10}$, 11057-43-5; $(Ph_2C_2)Co_2(CO)_3[P(OMe)_3]_3$, 55925-87-6; $[(CF_3)_2C_2]Co_2(CO)_3[P(OMe)_3]_3$, 90219-89-9.

Contribution from the Department of Chemistry, Miami University, Oxford, Ohio 45056

Electronic Structure of $(\mu\text{-H})Cr_2(CO)_{10}^-$

CHARLES J. EYERMANN and ALICE CHUNG-PHILLIPS*

Received October 18, 1983

Ground-state self-consistent-field Xα scattered-wave (SCF-Xα-SW) calculations have been carried out for the dinuclear transition-metal hydride complex $(\mu\text{-H})Cr_2(CO)_{10}^-$. Valence energy levels and sphere charge distributions, core energy levels, and total energies and sphere charges are obtained. The principal MO describing the Cr–H–Cr bond, $15a_1$, is predominantly H ligand in character. Other MOs with noticeable H ligand character include $7a_1$, $8a_1$, $9a_1$, and $14a_1$. These findings indicate that the bonding scheme for the Cr–H–Cr linkage is more complex than the qualitative three-center two-electron bond previously proposed. One of the two highest occupied MOs, $16b_1$, is Cr–Cr antibonding and $Cr–CO_t$ bonding where CO_t refers to the trans carbonyl. The lowest lying virtual orbital, $18a_1$, is Cr–Cr bonding but both $Cr–CO_t$ and $H–Cr_2$ antibonding. The lowest energy electronic transition, $16b_1 \rightarrow 18a_1$, is therefore expected to produce an excited state that is conducive to a facile CO dissociation but is not favorable to the disruption of the Cr–H–Cr bridging framework. This excited state is consistent with the high quantum yield observed for the photosubstitution of CO and the low quantum yield for photoinduced dimer disruption.

Introduction

In 1970, the geometry of the non-hydrogen framework in the anion of $[Et_4N^+][(\mu\text{-H})Cr_2(CO)_{10}^-]$, determined by X-ray diffraction,[1] was used to postulate a linear M–H–M bridging unit, **1**, where M designates the metal. However, X-ray and

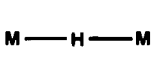

1

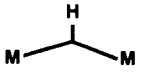

2

subsequent neutron diffraction investigations[2] on $(\mu\text{-H})W_2(CO)_9NO$ supplied the first direct evidence that unsupported M–H–M linkages are inherently bent, **2**. Indeed, a reinvestigation of $[Et_4N^+][(\mu\text{-H})Cr_2(CO)_{10}^-]$ using neutron diffraction revealed the H ligand position to be ca. 0.3 Å above the Cr–Cr internuclear axis;[3] i.e., the Cr–H–Cr fragment in this complex is *bent* and not linear as originally suggested. Additional X-ray and neutron diffraction studies have reaffirmed the bent configuration of M–H–M and have also shown that M–H–M bond angles may vary from 85 to 159°.[4] For example, the Et_4N^+ and Ph_4P^+ salts of $(\mu\text{-H})W_2(CO)_{10}^-$ have W–H–W bond angles of 137 and 123°, respectively.[4c] The highly variable M–H–M angle suggests an easily deformable M–H–M bridge.

Based on the neutron diffraction study[2b] of $(\mu\text{-H})W_2(CO)_9NO$, the H position is displaced outward from (**3**), rather than at (**4**), the intersection of the metal–axial-ligand (M–L) bond vectors. The observation has led to the supposition that

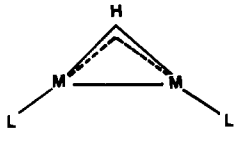

3

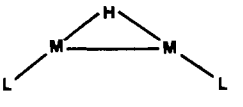

4

the M–H–M bond is best described as a closed (**5**), rather than an open (**6**), three-center two-electron (3c, 2e) bond.

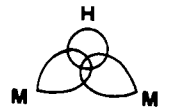

5

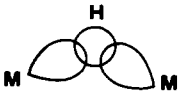

6

(1) Handy, L. B.; Ruff, J. K.; Dahl, L. F. *J. Am. Chem. Soc.* **1970**, *92*, 7312.

(2) (a) Andrews, M. A.; Tipton, D. L.; Kirtley, S. W.; Bau, R. *J. Chem. Soc., Chem. Commun.* **1973**, 181. (b) Olsen, J. P.; Koetzle, T. F.; Kirtly, S. W.; Andrews, M. A.; Tipton, D. L.; Bau, R. *J. Am. Chem. Soc.* **1974**, *96*, 6621.

(3) Roziere, J.; Williams, J. M.; Stewart, R. P., Jr.; Petersen, J. L.; Dahl, L. F. *J. Am. Chem. Soc.* **1977**, *99*, 4497.

(4) (a) Petersen, J. L.; Johnson, P. L.; O'Connor, J.; Dahl, L. F. *Inorg. Chem.* **1978**, *17*, 3460. (b) Petersen, J. L.; Brown, R. K.; Williams, J. M.; McMullan, R. K. *Ibid.* **1979**, *18*, 3493. (c) See references cited in: Bau, R.; Teller, R. G. *Struct. Bonding (Berlin)* **1981**, *44*, 1.

0020-1669/84/1323-2025$01.50/0

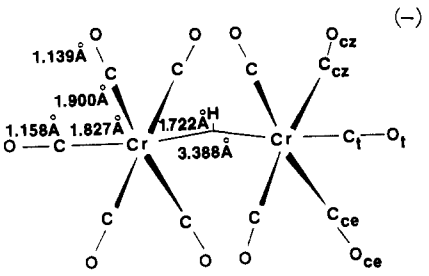

Figure 1. Geometry of $(\mu\text{-H})Cr_2(CO)_{10}^-$.

Table I. Geometric Coordinates and Sphere Radii (a_0) for $(\mu\text{-H})Cr_2(CO)_{10}^-$

region	x	y	z	radius
H	0.0	0.0	0.5958	1.4958
Cr	±3.1993	0.0	0.0	2.1440
C_t	±6.6519	0.0	0.0	1.6221
O_t	±8.8364	0.0	0.0	1.6307
C_{cz}	±3.1993	±2.5255	2.5255	1.6109
O_{cz}	±3.1993	±4.0448	4.0448	1.6167
C_{ce}	±3.1993	±2.5255	−2.5255	1.6112
O_{ce}	±3.1993	±4.0448	−4.0448	1.6167
outer	0.0	0.0	0.0	10.4671

Adoption of the bonding scheme depicted in **3** and **5** implies a significant metal–metal interaction in the bridging bond. Photochemically, the process of dimer disruption in $(\mu\text{-H})Cr_2(CO)_{10}^-$ is not very efficient,[5] supporting the idea that the M–M interaction is important. More recently, the photoelectron spectra of numerous metal hydride carbonyl clusters including $(\mu\text{-H})_3Mn_3(CO)_{12}$, $(\mu\text{-H})_3Re_3(CO)_{12}$, $(\mu\text{-H})_2Os_3(CO)_{10}$, and $(\mu\text{-H})_4Os_4(CO)_{12}$ have been reported;[6-8] ionization potentials (IPs) related to the M–H–M bonds in these complexes are used to argue for a (3c, 2e) bond with a high degree of H ligand localization.[7] To some extent theoretical descriptions of the bridging bond still rely on qualitative schemes analogous to the bonding formalisms already established for boron hydrides,[4c,7a,9] although more quantitative molecular orbital (MO) calculations are now emerging.[8]

As part of our theoretical studies on transition-metal hydrides,[10] the electronic structure of the dinuclear hydride complex $(\mu\text{-H})Cr_2(CO)_{10}^-$ has been investigated by the self-consistent-field Xα scattered-wave (SCF–Xα–SW) method. A particular emphasis is placed on the elucidation of the nature of the Cr–H–Cr linkage and the correlation of calculated results with the aforementioned photochemical and photoelectron data on the M–H–M bond.

Computational Details

The Xα–SW method has been thoroughly described in standard references.[11] Computationally, $(\mu\text{-H})Cr_2(CO)_{10}^-$ is an extremely large system (with 23 atoms and 190 electrons); details germane to this study will be discussed briefly.

The neutron diffraction geometry[4] of the chosen anion in its Et_4N^+ salt was idealized to C_{2v} symmetry. A schematic drawing of the geometry of this ion is shown in Figure 1. There are eight cis and two trans carbonyls. The four cis CO's on the same side of the Cr–Cr internuclear axis as the H ligand are labeled as CO_{cz}; the four on the opposite side are CO_{ce}. The two trans CO's are simply CO_t. Coordinates of the atoms and the center of outer sphere are presented in Table I.

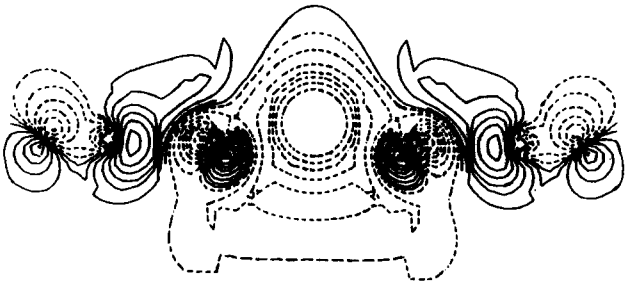

Figure 2. Contour plots on the xz plane for the $15a_1$ molecular orbital of $(\mu\text{-H})Cr_2(CO)_{10}^-$. The contour values in $a_0^{-3/2}$, starting from the outermost to the innermost, are ±0.0075, ±0.0200, ±0.0400, ±0.0800, ±0.1000, and ±0.1250.

Schwarz's α values were used for all atoms except the H atom, for which 0.777 25 was employed.[12] The α value for the intersphere, taken to be the same as the outer sphere, was calculated as the valence-electron weighted average of all atomic α values. The initial molecular potential was generated by a superposition of SCF–Xα charge densities for the free Cr and C atoms and for the free $O^{0.1-}$ species as a result of assigning the negative charge of the anion to the ten highly electronegative O atoms. The 1s radial function of the free H atom was used for the H ligand. A Watson sphere[11b] with a radius equal to the outer sphere and with 1 unit of positive charge uniformly distributed over its surface was used to simulate the crystalline environment[13] of the anion in $[Et_4N^+][(\mu\text{-H})Cr_2(CO)_{10}^-]$.

For the partial-wave expansion, spherical harmonics through l = 4 for the outer sphere, l = 2 for the two Cr, l = 1 for the C and O, and l = 0 for the H regions were used, leading to a secular determinant of order 124. Linear combinations of spherical harmonics were next obtained to form symmetry-adapted bases for the symmetry species of the C_{2v} point group. By means of the new bases the original determinant was reduced to a block-diagonal form with component determinants of lower orders 38 (A_1), 25 (A_2), 34 (B_1), and 27 (B_2), where the symmetry species is indicated in parentheses.

The method of Norman[14] was used to determine the atomic sphere radii, which were chosen as 88% of the atomic-number sphere radii; their values are also presented in Table I. This choice of radii led to two nonoverlapping Cr spheres and ca. 12% overlap between each Cr and the H spheres.

In the SCF calculation, a 9:1 ratio of old to new potentials for a given iteration was used as the starting potential for the next iteration. The Cr 1s, 2s, 2p, 3s, and 3p orbitals were treated as core orbitals; i.e., their potentials were constructed by using only the charge density inside the Cr atomic sphere. The C and O 1s orbitals were treated similarly. The core energy levels were not frozen, as they were computed in each iteration. It should be noted that due to the large size and low symmetry of the complex, several problems arose in the search for eigenvalues and were subsequently resolved.[10]

The ground-state orbital eigenvalues converged to better than ±0.000 05 hartree in about 40 iterations on an IBM 370/148 computer. The entire SCF–Xα–SW calculation required ca. 29 CPU hours.

Ground-State Molecular Orbitals, Energies, and Charges

For the ground state of $(\mu\text{-H})Cr_2(CO)_{10}^-$, Xα–SW valence energy levels and sphere charge distributions are given in Table II and total energies and sphere charges in Table III. The particular choice of atomic sphere radii has yielded a virial theorem ratio of 1.0012 (Table III).[14] Available as supplementary material are Xα–SW results for the low-lying valence

(5) Darensbourg, D. J.; Incorvia, M. J. *Inorg. Chem.* **1979**, *18*, 18.
(6) Wong, K. S.; Dutta, T. K.; Fehlner, T. P. *J. Organomet. Chem.* **1981**, *215*, C48.
(7) (a) Green, J. C.; Mingos, D. M. P.; Seddon, E. A. *J. Organomet. Chem.* **1980**, *185*, C20. (b) Green, J. C.; Mingos, D. M. P.; Seddon, E. A. *Inorg. Chem.* **1981**, *20*, 2595.
(8) (a) Sherwood, D. E., Jr.; Hall, M. B. *Inorg. Chem.* **1982**, *21*, 3458. (b) See references cited in: Chesky, P. T.; Hall, M. B. *Ibid.* **1983**, *22*, 3327.
(9) Harris, D. C.; Gray, H. B. *J. Am. Chem. Soc.* **1975**, *97*, 3073.
(10) Eyermann, C. J. Ph.D. Dissertation, Miami University, Oxford, OH, 1981.
(11) See, e.g.: (a) Connolly, J. W. D. In "Semiempirical Methods of Electronic Structure Calculation. Part A: Techniques"; Segal, G. A. Ed.; Plenum Press: New York, 1977; pp 105–132. (b) Slater, J. C. "The Calculation of Molecular Orbitals"; Wiley: New York, 1979.
(12) (a) Schwarz, K. *Phys. Rev. B: Solid State* **1972**, *5*, 2466; *Theor. Chim. Acta* **1974**, *34*, 225. (b) Slater, J. C. *Int. J. Quantum Chem.* **1973**, *7S*, 533.
(13) Handy, L. B.; Treichel, P. M.; Dahl, L. F.; Hayter, R. G. *J. Am. Chem. Soc.* **1966**, *88*, 366.
(14) Norman, J. G., Jr. *J. Chem. Phys.* **1974**, *61*, 4630; *Mol. Phys.* **1976**, *31*, 1191.

Table II. Valence Energy Levels (hartrees) and Sphere Charge Distributions for $(\mu\text{-H})Cr_2(CO)_{10}^-$

			percent charge in various spheres							
level	energy[a]	type	H	2Cr	$2C_t$	$2O_t$	$4C_{cz}$	$4O_{cz}$	$4C_{ce}$	$4O_{ce}$	inter
$12a_2$	−0.2193	3d		64	3	5	1	2	3	3	19
$16b_1$	−0.2193	3d		64	3	5	1	3	1	3	20
$15b_1$	−0.2248	3d		61	0	0	3	7	3	7	19
$17a_1$	−0.2264	3d	0	59	2	5	1	2	2	6	23
$16a_1$	−0.2272	3d	0	60	0	0	2	7	2	7	22
$12b_2$	−0.2288	3d		60	2	5	1	4	1	4	23
$15a_1$	−0.3948	HCr_2	23	8	10	3	12	8	7	5	24
$11a_2$	−0.4041	5σ		6	0	4	25	6	25	7	27
$14b_1$	−0.4041	5σ		6	0	4	25	6	25	7	27
$11b_2$	−0.4094	5σ		6	1	5	24	7	24	8	25
$14a_1$	−0.4155	5σ	8	6	6	4	15	14	16	6	25
$13b_1$	−0.4398	1π		3	6	1	4	11	14	39	22
$10a_2$	−0.4406	1π		0	0	0	7	21	12	36	24
$9a_2$	−0.4407	1π		0	0	5	2	6	17	46	24
$12b_1$	−0.4414	1π		1	4	14	12	36	3	8	22
$8a_2$	−0.4417	1π		0	2	8	18	49	0	0	23
$10b_2$	−0.4423	1π		0	0	0	9	26	11	31	23
$13a_1$	−0.4481	1π	0	0	8	24	5	14	7	19	23
$9b_2$	−0.4481	1π		0	8	23	7	16	6	17	23
$11b_1$	−0.4516	1π		0	2	6	10	21	11	24	26
$7a_2$	−0.4517	1π		1	2	6	11	25	9	21	25
$8b_2$	−0.4526	1π		0	0	0	10	27	12	27	24
$12a_1$	−0.4586	1π	1	3	1	0	8	9	15	36	27
$7b_2$	−0.4602	1π		2	0	0	13	24	12	20	29
$10b_1$	−0.4624	1π		2	0	1	12	25	11	23	26
$11a_1$	−0.4654	1π	0	2	2	0	10	21	12	25	28
$6a_2$	−0.4668	1π		2	14	30	6	7	6	7	28
$9b_1$	−0.4668	1π		2	14	30	7	8	6	6	27
$10a_1$	−0.4679	1π	1	2	11	24	26	8	9	11	29
$6b_2$	−0.4683	1π		2	12	26	7	8	10	6	29
$9a_1$	−0.4719	1π	8	4	3	2	16	32	3	2	30
$5a_2$	−0.4774	5σ		29	0	0	24	2	24	2	19
$8b_1$	−0.4789	5σ		23	35	3	7	2	7	2	19
$5b_2$	−0.4801	5σ		28	0	0	25	2	24	2	19
$8a_1$	−0.4880	5σ	5	27	23	2	8	1	13	3	18
$7b_1$	−0.5170	5σ		13	11	2	19	3	19	3	30
$7a_1$	−0.5379	5σ	11	14	12	3	14	3	11	2	30

[a] Xα–SW orbital eigenvalue as defined in ref 11.

Table III. Total Energies (hartrees) and Sphere Charges (electrons) in $(\mu\text{-H})Cr_2(CO)_{10}^-$

total energy (E)	−3220.0843
kinetic energy (T)	3227.7684
potential energy (V)	−6447.8528
virial theorem ratio ($-2T/V$)	1.0012
intersphere potential energy	−0.2486

	sphere charge		sphere charge
H	1.1483	each O_{cz}	7.6195
each Cr	23.6450	each C_{ce}	5.3536
each C_t	5.3423	each O_{ce}	7.6209
each O_t	7.6961	intersphere	11.6266
each C_{cz}	5.3479	extramolecular	0.0905

energy levels (those at ca. −1.3 and −0.64 hartrees composed essentially of the unperturbed 3σ and 4σ orbitals of the CO ligands) and the core orbitals.

The valence MOs in Table II can be conveniently grouped into two regions according to their energies and characters. The MOs between −0.55 and −0.40 hartree can be classified as Cr–C σ-bonding orbitals derived from Cr orbitals and the 5σ orbitals of the CO ligands and as those derived principally from the 1π orbitals of the CO ligands. Finally, the upper valence MOs, located between −0.40 and −0.20 hartree, consist of the $(\mu\text{-H})Cr_2$ bonding MO ($15a_1$) and the three pairs of bonding and antibonding combinations of the 3d orbitals on the two Cr atoms ($12b_2$ vs. $12a_2$, $16a_1$ vs. $15b_1$, and $17a_1$ vs. $16b_1$). Note especially that the highest occupied MOs (HOMOs) are $16b_1$ and $12a_2$, which have nearly identical energies.

The $15a_1$ MO is the principal component of the Cr–H–Cr bond. A contour diagram for $15a_1$ is shown in Figure 2. The atomic sphere charge distributions indicate that this MO is mainly H ligand in character. The small amount of charge contained inside the Cr atomic spheres is essentially associated with the Cr 4p orbitals. Further discussions on the nature of the Cr–H–Cr bond will focus on the charge localized on the H ligand as well as the strength of the Cr–Cr interaction.

H Ligand Charge

The C_{2v} geometry of $(\mu\text{-H})Cr_2(CO)_{10}^-$ restricts the participation of the H ligand to only MOs belonging to the A_1 symmetry species. Among the MOs listed in Table II, only $7a_1$, $8a_1$, $9a_1$, $14a_1$, and $15a_1$ contribute noticeably to the total integrated charge of 1.15 electrons inside the H atomic sphere as given in Table III. Clearly, the principal component of the Cr–H–Cr bond, $15a_1$, has the highest percentage of the total *H atomic sphere charge* (ca. 40%). The other MOs in decreasing importance are $7a_1$ (19%), $9a_1$ (14%), $14a_1$ (14%), and $8a_1$ (9%). The final 4% of the charge is contributed by the remaining MOs of A_1 species. Adding to the H atomic sphere charge the amount partitioned from the intersphere and extramolecular regions by using the valence-electron weighted scheme of Norman[15] yields a total of 1.25 electrons for H, or a value of 0.25− as the atomic charge for H, Q^H.

Cognizant of the recent studies on H ligand charges in mononuclear hydride complexes[16,17] using the projected Xα (PXα) method,[18] we expect the Q^H value of 0.25− predicted

(15) Norman, J. G., Jr. *Inorg. Chem.* **1977**, *16*, 1028.
(16) Eyermann, C. J.; Chung-Phillips, A., submitted for publication in *J. Am. Chem. Soc.*
(17) Eyermann, C. J.; Chung-Phillips, A. *J. Chem. Phys.*, in press.
(18) Bursten, B. E.; Fenske, R. F. *J. Chem. Phys.* **1977**, *67*, 3138.

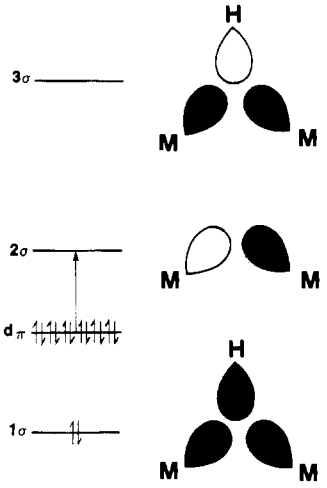

Figure 3. Simple bonding model for the three-center two-electron M–H–M bond. Adapted from (a) ref 9 and (b) ref 5.

by Norman's method to be correct in sign but significantly too low in magnitude. Experimental evidence supporting a relatively high negative charge on the H ligand in this ion is provided by the IPs of MOs involving the M–H–M fragments in related bridging hydrides.[6-8] These IPs are found to be ca. 12 eV, which is significantly greater than the 7.5–9.0 eV ascribed to an IP related to a M–M bond. The increase in IP values is attributed[7] to a M–H–M bond predominantly H in character.

A previous theoretical study has asserted that 90% of the ^{1}H chemical shift in transition-metal hydrides such as $HCo(CO)_4$, $H_2Fe(CO)_4$, and $HIr(CN)_5^{3-}$ is due to the charge on the H ligand.[19] The observed shifts for the isoelectronic pair of molecules, $HMn(CO)_5$ and $HCr(CO)_5^-$, are τ 17.5 and 17.0, respectively.[20] This similarity in ^{1}H chemical shift implies an analogous similarity in Q^H; i.e., the Q^H for $HCr(CO)_5^-$ must be close to the Q^H value of 0.26– reported previously[17] for $HMn(CO)_5$. $(\mu\text{-H})Cr_2(CO)_{10}^-$, on the other hand, has a shift of τ 29.5, which is considerably larger than τ 17.0 observed for $HCr(CO)_5^-$.[20] Since $(\mu\text{-H})Cr_2(CO)_{10}^-$ is formed by the reaction of $HCr(CO)_5^-$ with the neutral $HCr(CO)_5$, the dramatic increase of τ 12.5 implies a considerable increase in the magnitude of Q^H on going from $HCr(CO)_5^-$ to the dinuclear complex. The Q^H for $(\mu\text{-H})Cr_2(CO)_{10}^-$ is therefore expected to be more negative than 0.26–, the value ascribed to $HCr(CO)_5^-$.

To summarize, there is ample experimental evidence to support a high negative charge on the H ligand in this complex. The Q^H value of 0.25– predicted by Norman's method should represent a lower limit. In a previous study,[17] a discrepancy of 0.3 has been found for the Q^H in $H_2Fe(CO)_4$ between values determined by Norman's method (0.04–) and the PXα analysis (0.33–). If Norman's method yields a Q^H value of 0.25– in $(\mu\text{-H})Cr_2(CO)_{10}^-$, the correct value may well be as high as 0.4– or even 0.5–.

Cr–Cr Interaction

The Xα–SW results show that the charge on the H ligand of $(\mu\text{-H})Cr_2(CO)_{10}^-$ is distributed among the $7a_1$, $8a_1$, $9a_1$, $14a_1$, and $15a_1$ MOs. This involvement of H in more than one MO indicates that the bonding scheme for the Cr–H–Cr linkage is more complex than the qualitative bonding scheme in Figure 3 for a (3c, 2e) M–H–M bond, proposed by Harris and Gray[9] to account for the electronic spectrum of $(\mu\text{-H})W_2(CO)_{10}^-$. To provide a comparison with Figure 3 and to facilitate the following discussion, contour diagrams for the

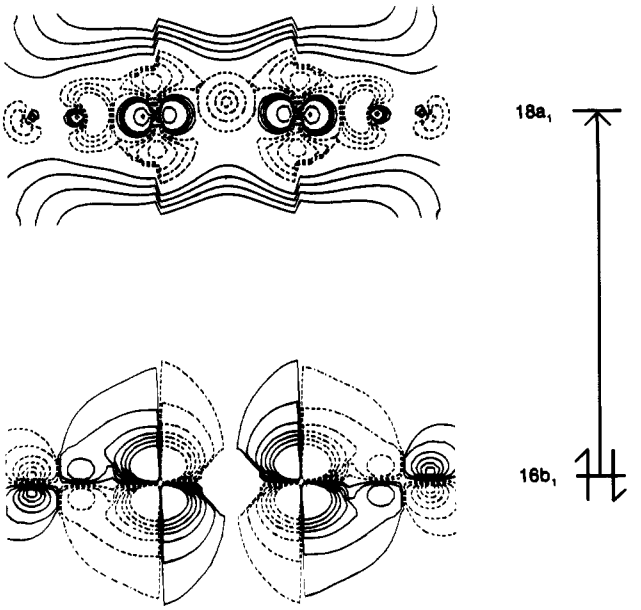

Figure 4. Contour plots on the *xz* plane for the $16b_1$ molecular orbital and the $18a_1$ virtual orbital of $(\mu\text{-H})Cr_2(CO)_{10}^-$. Also depicted is the lowest energy electronic transition, $16b_1 \rightarrow 18a_1$. The contour values for $16b_1$ are the same as those specified in the caption for Figure 2. Those for $18a_1$ are ±0.0025, ±0.0050, ±0.0075, ±0.0100, ±0.0300, ±0.0500, ±0.0700, ±0.0900, and ±0.1100.

Xα–SW HOMO, $16b_1$, and the lowest lying virtual orbital, $18a_1$, are presented in Figure 4.

With respect to both character and ordering of energy levels, there are correspondences between the 1σ orbital in Figure 3 and the Xα–SW $15a_1$ MO in Figure 2 and between the six degenerate HOMOs, d_π, in Figure 3 and the six uppermost MOs ($12b_2$–$12a_2$) in Table II. The two schemes differ in the character of their respective lowest unoccupied MOs (LUMOs). The LUMO in Figure 3, 2σ, is M–M antibonding and contains no H character due to symmetry restrictions. Yet, the Xα–SW LUMO, $18a_1$ in Figure 4, is Cr–Cr bonding but antibonding with respect to both H–Cr_2 and Cr–CO_t interactions. In view of this character, $18a_1$ would correspond to the 3σ, rather than the 2σ, of Figure 3. (It should be noted that $18a_1$ is not the antibonding counterpart of $15a_1$ but is more likely the antibond of $8a_1$ on the basis of an orbital contour analysis.[10])

The character of $18a_1$ allows both a rational deduction of the strength of the Cr–Cr interaction and a more satisfactory interpretation of the observed photochemistry.[5] Foremost in importance is the fact that $18a_1$ is the LUMO, the most stable of the virtual orbitals, in spite of the H–Cr_2 and Cr–CO_t σ-antibonding interactions. The stability of $18a_1$, therefore, must be due to the greater strength of the Cr–Cr bonding interaction. This postulation is supported by the observed quantum yields of 0.036 and 0.20 for the respective dimer disruption and CO photosubstitution in $(\mu\text{-H})Cr_2(CO)_{10}^-$ under the irradiation of 410-nm light.[5] The photochemical findings clearly suggest that an electronic transition into the LUMO will produce an excited state that is conducive to a facile CO dissociation but is not favorable to the disruption of the Cr–H–Cr bridging framework.

The qualitative energy-level diagram shown in Figure 3 indicates that the lowest energy electronic transition, $d_\pi \rightarrow 2\sigma$, will populate a M–M antibonding orbital. If the M–M interaction is indeed important, then this bonding scheme will suggest the dimer disruption to be a favorable process. According to the Xα–SW calculation, the lowest energy electronic transition (as depicted in Figure 4) is $16b_1 \rightarrow 18a_1$, where $16b_1$ is Cr–Cr antibonding but Cr–CO_t bonding. This transition,

(19) Lohr, L. L., Jr.; Lipscomb, W. N. *Inorg. Chem.* **1964**, *3*, 22.
(20) Darensbourg, M. Y.; Deaton, J. C. *Inorg. Chem.* **1981**, *20*, 1644.

which simultaneously depopulates a Cr–Cr antibonding orbital and populates a Cr–Cr bonding orbital, will then strengthen the Cr–Cr interaction in opposition to a dimer disruption. From the low quantum yield for dimer disruption in $(\mu\text{-H})Cr_2(CO)_{10}^-$ and the Cr–Cr bonding feature of the Xα–SW LUMO $18a_1$, one must conclude that the Cr–Cr bonding interaction in the lowest excited state of this complex is significant.

The $16b_1 \rightarrow 18a_1$ transition is also consistent with the high quantum yield observed for the photosubstitution of CO. This transition depopulates $16b_1$ and thus weakens the σ-bonding between the Cr $3d_\pi$ and CO 2π orbitals; the effect is enhanced by populating $18a_1$, which is clearly $Cr–CO_t$ σ-antibonding. It is interesting to note that the $d_\pi \rightarrow 2\sigma$ transition deduced from the simple bonding scheme in Figure 3 also permits a facile CO dissociation as the d_π orbitals are depopulated.

So far as the photodissociation of CO is concerned, an apparent anomaly exists between the Xα–SW prediction of a trans-CO dissociation and the observed substitution of a cis CO. A plot of $18a_1$ in a xy plane containing four cis CO's and one Cr reveals that the CO's are σ-bonding to the Cr.[10] Therefore, a $16b_1 \rightarrow 18a_1$ transition should not directly effect a cis-CO dissociation. Experimentally, it is known that complexes like $(\mu\text{-H})Cr_2(CO)_{10}^-$ are very fluxional; thus it is conceivable that a trans CO is lost upon irradiation, and a subsequent rearrangement of the resultant $HCr_2(CO)_9^-$ species takes place.[21] The event could then lead to a final product that appears to have originated from a cis-Co photodissociation.

Acknowledgment. We are indebted to Professor S. Doniach, Professor H. Schlosser, and Dr. D. K. Misemer for their valuable assistance with the Xα–SW programs. We also thank Professor J. G. Norman, Jr., for a very helpful correspondence.

Registry No. $(\mu\text{-H})Cr_2(CO)_{10}^-$, 73740-63-3.

Supplementary Material Available: Tables S-I (low-lying valence energy levels and sphere charge distributions) and S-II (core energy levels) for $(\mu\text{-H})Cr_2(CO)_{10}^-$ (1 page). Ordering information is given on any current masthead page.

(21) Darensbourg, D. J.; Murphy, M. A. *J. Am. Chem. Soc.* **1978**, *100*, 463; *Inorg. Chem.* **1978**, *17*, 884.

Contribution from the Department of Chemistry, University of New Brunswick, Fredericton, New Brunswick E3B 6E2, Canada

Gas-Phase Bihalide and Pseudobihalide Ions. An Ion Cyclotron Resonance Determination of Hydrogen Bond Energies in XHY^- Species (X, Y = F, Cl, Br, CN)

J. W. LARSON[1] and T. B. McMAHON*

Received August 30, 1983

Hydrogen bond energies in the homonuclear bihalide ions FHF^- and $ClHCl^-$, the mixed-bihalide ion $ClHF^-$, and the pseudobihalide ions $FHCN^-$ and $ClHCN^-$ have been determined from ion cyclotron resonance halide-exchange equilibria measurements. A correlation between shift in frequency in hydrogen bond motion relative to the free halogen acid and hydrogen bond strength is proposed, which allows prediction of hydrogen bond energies for the additional species $FHBr^-$, FHI^-, $ClHBr^-$, and $ClHI^-$. Empirical correlations of trends in hydrogen bond energies also allow predictions to be made for $BrHBr^-$, $BrHCN^-$, and $CNHCN^-$. Ab initio calculations have been used to determine that the shape of the potential energy well for proton motion in the bihalide ions is a single minimum one.

Introduction

The hydrogen bihalide ions, XHY^-, represent the simplest examples of strongly hydrogen-bonded species. Their linear, triatomic structure has made them readily amenable to structural characterization by neutron diffraction,[2,3] X-ray crystallographic,[4] and vibrational spectroscopic methods.[5-10] Many studies have shown that the bifluoride ion, FHF^-, is a linear, centrosymmetric anion, both in crystalline salts with alkali metals[2,3] and tetraalkylammonium cations[4] and under argon matrix isolation conditions.[11] Considerably less structural information has been available for the other homonuclear bihalide ions until recent matrix isolation studies by Ault and Andrews[12] and photoionization studies by Milligan and Jacox[9] and by Pimentel and co-workers.[8] Evans and Lo[5] found the infrared spectra of the bihalide ion to be very dependent on the environment of the ion. They postulated that the HCl_2^- and HBr_2^- ions existed in two forms, an asymmetric anion and a centrosymmetric species with a single minimum potential, the latter form being favored in solution and in salts with large cations. Under matrix isolation conditions, however, the only observable HCl_2^- or HBr_2^- anion is the centrosymmetric species.[8,9,12-14]

Much less was known about mixed-bihalide ions until recent argon matrix isolation experiments.[11,12,14] The results of these experiments have been interpreted as indicating that the XHY^- anions can exist in two spectroscopically detectable forms analogous to those of the homonuclear bihalides. The higher infrared absorption frequency has been assigned to a species with a double minimum potential well for the hydrogen bond stretching motion, while a lower frequency has been assigned to a species with a single minimum potential similar to the centrosymmetric anion of the symmetric bihalide anions. The

(1) On sabbatical leave from Marshall University, Huntington, WV.
(2) Ibers, J. A. *J. Chem. Phys.* **1964**, *40*, 402.
(3) McGaw, B. L.; Ibers, J. A. *J. Chem. Phys.* **1963**, *39*, 2677.
(4) McDonald, T. R. R. *Acta Crystallogr.* **1960**, *13*, 113.
(5) (a) Evans, J. C.; Lo, G. Y. S. *J. Phys. Chem.* **1967**, *71*, 3942. (b) Evans, J. C.; Lo, G. Y. S. *Ibid.* **1969**, *73*, 448. (c) Evans, J. C.; Lo, G. Y. S. *Ibid.* **1966**, *70*, 11.
(6) Nibler, J. W.; Pimentel, G. C. *J. Chem. Phys.* **1967**, *47*, 710.
(7) Salthouse, J. A.; Waddington, T. C. *J. Chem. Soc. A* **1966**, 28.
(8) (a) Noble, P. N.; Pimentel, G. C. *J. Chem. Phys.* **1968**, *49*, 3165. (b) Noble, P. N. *Ibid.* **1972**, *56*, 2088.
(9) (a) Milligan, D. E.; Jacox, M. E. *J. Chem. Phys.* **1970**, *53*, 2034. (b) Milligan, D. E.; Jacox, M. E. *Ibid.* **1971**, *55*, 2550.
(10) Ault, B. S. *Acc. Chem. Res.* **1982**, *15*, 103 and references contained therein.
(11) Ault, B. S. *J. Phys. Chem.* **1979**, *83*, 837.
(12) Ault, B. S.; Andrews, L. *J. Chem. Phys.* **1975**, *63*, 2466.
(13) Hunt, R. L.; Ault, B. S. *Spectrochem. Acta, Part A* **1981**, *37A*, 63.
(14) Ellison, C. M.; Ault, B. S. *J. Phys. Chem.* **1979**, *83*, 832.

0020-1669/84/1323-2029$01.50/0